Nonlinear Multiple Models Adaptive Secondary Voltage Control of Microgrids

Zixiao Ma, *Graduate Student Member, IEEE*, Zhaoyu Wang, *Member, IEEE*, Yifei Guo, *Member, IEEE*, Yuxuan Yuan, *Graduate Student Member, IEEE*, and Hao Chen, *Member, IEEE*

***Abstract*—This article proposes a model-free secondary voltage control (SVC) for microgrids (MG) using nonlinear multiple models adaptive control. Firstly, a linear robust adaptive controller is designed to guarantee the voltage stability in the bounded-input-bounded-output (BIBO) manner so as to meet the operation requirements of MGs. Secondly, a nonlinear adaptive controller is developed to improve the voltage tracking performance with the help of artificial neural networks (ANNs). A switching mechanism for coordinating such two controllers is designed to guarantee the closed-loop stability while achieving accurate voltage tracking. By an online identification based on the input and output data of MGs, the proposed method does not resort to any *apriori* information of system model and primary control, thus exhibiting good robustness, ease of deployment and disturbance rejection.**

***Index Terms*—Artificial neural network (ANN), microgrid (MG), multiple models, adaptive control, secondary voltage control (SVC).**

NOMENCLATURE

Abbreviations

ANN	Artificial neural network
BIBO	Bounded-input bounded-output
DER	Distributed energy resource
LAC	Linear adaptive controller
ARMAX	Auto-regressive moving average with exogenous input model
MG	Microgrid
MGCC	Microgrid central controller
NAC	Nonlinear adaptive controller
PI	Proportion-Integral
PV	Photovoltaic
SVC	Secondary voltage control
SNR	Signal-to-noise ratio.

Variables

J	Objective function
$\boldsymbol{E}^*$	Vector of voltage reference from SVC
$\boldsymbol{e}_L, \boldsymbol{e}_N$	Error vectors of linear and nonlinear models
$\bar{\boldsymbol{e}}$	Voltage tracking error vector
$\boldsymbol{h}$	Linear-transformed unmodeled dynamics
$\delta\boldsymbol{h}, \delta\hat{\boldsymbol{h}}$	Residual between real voltage and estimated voltage and its estimation using ANN
k	Time step index
$\boldsymbol{v}_o^{\text{ref}}$	Predefined voltage reference
$\boldsymbol{v}_o$	Vector of voltage magnitude
v_{oi}	Terminal voltage magnitude of the ith DER
v_{odi}, v_{oqi}	dq components of v_{oi}
$\hat{\boldsymbol{W}}$	Estimation of the ideal weight matrix
$\boldsymbol{\Psi}, \bar{\boldsymbol{\Psi}}$	Vector of output and input voltage and its rearrangement
$\boldsymbol{y}$	Linear transformed output voltage vector
$\hat{\boldsymbol{y}}_L, \hat{\boldsymbol{y}}_N$	Estimated transformed output voltage vectors using linear and nonlinear model identifier
Δ	Positive constant
ϵ	Small positive constant
μ	Non-negative constant
$\boldsymbol{\Phi}$	Unmodeled dynamics
$\boldsymbol{x}$	Compact state variable vector of a MG
$\boldsymbol{\psi}_i$	State vector of the ith DER
ξ	Performance index of switching mechanism.

Parameters

$\boldsymbol{A}(\cdot)$	Matrix polynomial of nth-order backward shift operator
$\boldsymbol{B}(\cdot)$	Matrix polynomial of $(n-1)$th-order backward shift operator
d	Relative degree
$\boldsymbol{F}(\cdot)$	Diagonal and stable weight matrix polynomial
$\boldsymbol{K}(\cdot), \boldsymbol{L}(\cdot)$	Matrix polynomials of $(n-1)$th-order
m	Number of DERs
n	MG system order
$\boldsymbol{R}$	Diagonal real matrix
ρ	Bound of magnitude of unmodeled dynamics
$\boldsymbol{\theta}$	Input-output parameter matrix
$\hat{\boldsymbol{\theta}}_L, \hat{\boldsymbol{\theta}}_N$	Estimated parameter matrices using linear and nonlinear models
ΔT	Sampling time of secondary control.

Manuscript received December 26, 2019; revised April 6, 2020 and July 16, 2020; accepted September 7, 2020. Date of publication September 10, 2020; date of current version December 21, 2020. This work was supported by the U.S. Department of Energy Wind Energy Technologies Office under Grant DE-EE0008956. Paper no. TSG-01929-2019. *(Corresponding author: Zhaoyu Wang.)*

Zixiao Ma, Zhaoyu Wang, Yifei Guo, and Yuxuan Yuan are with the Department of Electrical and Computer Engineering, Iowa State University, Ames, IA 50011 USA (e-mail: zma@iastate.edu; wzy@iastate.edu; yifeig@iastate.edu; yuanyx@iastate.edu).

Hao Chen is with Power Electronics Department, Tesla, Palo Alto, CA 94304 USA (e-mail: haochengt16@gmail.com).

Color versions of one or more of the figures in this article are available online at https://ieeexplore.ieee.org.

Digital Object Identifier 10.1109/TSG.2020.3023307

Sets

Ω	Set of linear parameter matrix polynomials
$\mathbb{R}$	Set of real numbers.

I. Introduction

MICROGRIDS (MGs) are localized small-scale power systems consisting of interconnected loads and distributed energy resources (DERs), which can operate in both grid-connected and islanded modes. Compared with traditional fossil-fuel-based power grids, they have the advantages of fast demand response, low-carbon consumption, flexible utilization of DERs and high self-healing capability, etc [1], [2].

Despite of many benefits, MGs also bring some new control challenges. One of the key issues is the voltage tracking in the islanded mode. As known, *hierarchical control* is a popular choice for MGs, in which the *primary voltage control* with fast response maintains the stability while the *secondary voltage control (SVC)* corrects the voltage deviations [1], [2].

As per the control architecture and communication requirements, MG control methods can be classified into three main categories: centralized, decentralized and distributed [3]. Centralized approaches are usually implemented with a microgrid central controller (MGCC) and point-to-point communication network. It has well served the industry for decades and performs many practical merits. For instance, they are easy to implement and house and often less costly for small-scale systems [4]. Moreover, centralized architecture provides the best foundation for advanced control applications since all relevant data can be collected and processed in a single controller. However, it may suffer from single point of failure [5]. Redundant communication systems can be installed to enhance the reliability; nonetheless, it will lead to additional cost [6]. Another solution is using decentralized or distributed control approaches. Decentralized control is implemented with local SVC controllers without communication network, assuming that the interactions between subsystems are negligible. However, this assumption does not always hold and might result in poor system-wide performance. Distributed control consists of local controllers and a sparse communication network. Averaging-based and consensus-based distributed SVC have been well investigated [7]. In the averaging-based SVC, each DER measures its required data and transmits them to all the other units [8]. The SVC signal is then calculated by averaging the received data from other DERs [9]. By employing the broadcast gossip algorithm, the required communication links can be reduced and the algorithm can converge to an equilibrium [10]. In the consensus-based SVC, the communication network is reduced more by transferring the required data just among the neighbor DERs [11]–[13].

Conventional SVC methods are based on *apriori* accurate models [14]. The input-output feedback linearization control [15] that builds on the full knowledge of MG models and primary control might contradict the concept of hierarchical control. Any changes of system structure or parameters could affect the control performance and could even result in instability. Some nonlinear control methods, e.g., model predictive control [16], sliding mode control [17], internal model control [18], also have similar drawbacks. Several SVC strategies are designed based on specified models of primary controllers and inner controllers [3], [19]–[21], which restricts their generalization. A finite-time control-based method [22] was proposed to overcome such drawback. To alleviate the dependence on accurate models, robust control [23], predictive control [24], and variable-structure control [25] methods have been investigated. To overcome time-varying communication delays and communication noise disturbances, robust secondary control approaches have been studied in [26], [27]. However, partial model and uncertainty dynamics are still required for robust control and variable-structure control, though they do improve robustness.

Recently, *model-free* control has attracted a lot of attention due to its advantages of robustness and flexibility [28]. Reference [29] proposed a data-driven adaptive voltage control scheme for interlinking converters in interlinked hybrid ac/dc MGs, where the inner loop adopts a data-driven adaptive voltage control and the SVC is essentially a Proportion-Integral (PI) controller. In [30], a bi-level distributed voltage control scheme was proposed, where the high-level controller is designed for loss minimization; the low-level controller regulates the power output and terminal voltage. In [31], a model-free sliding mode control was adopted where the parameters are tuned with heuristic techniques, nevertheless, it suffers from chattering problem due the nature of sliding mode control [32]. Distributed averaging-based PI controllers for secondary frequency and voltage control were developed in [8], [9], [33]; however, they still require MG network information for controller parameter design.

Though most of SVC methods establish on linearized [5], [7], [11], [19] or nonlinear system models [3], [12], [20], [21], unfortunately, the detailed MG information including network topology, line impedances and loads, may be fully or partially unavailable to establish accurate models in some cases. Moreover, since there are uncertainty dynamics and disturbances in DER-rich MGs, it is very hard to precisely capture such dynamics [34], [35]. Clearly, models with poor accuracy can significantly deteriorate the control performance. For the existing model-free control methods, they mostly resort to PI control, which often suffers from high starting overshoot, high sensitivity to controller gains and sluggish response to disturbances [36].

Our Contribution: To address these challenges, we propose a multi-variable robust adaptive SVC method for MGs, which builds on the *multiple models* and *artificial neural networks (ANNs)* that are exploited to estimate the unmodeled dynamics of MGs. The controller consists of two separate linear and nonlinear modes that are coordinated by a tailored switching strategy. In normal operation, the SVC operates under the nonlinear control mode which achieves the accurate voltage tracking. It will switch to the linear control mode so as to guarantee the stability once there are large disturbances. The proposed method is inherently model-free, in the sense that it does not rely on *apriori* knowledge of MG topology, line impedances and load demands, which enables independent designs between different control layers while enhancing

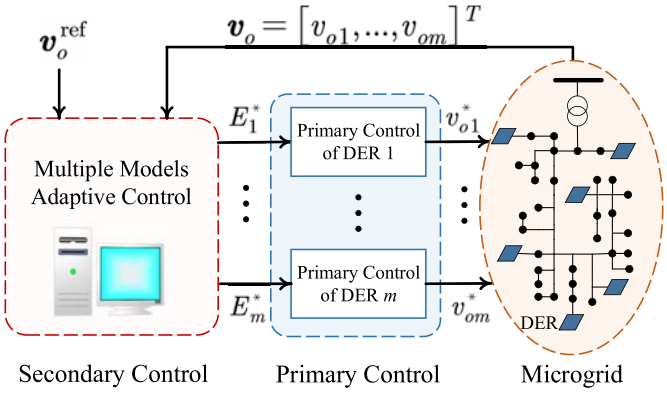

Fig. 1. Diagram of secondary and primary control structure of MG.

the robustness against uncertainties. We rigorously prove the global *bounded-input-bounded-output (BIBO)* stability of the controller and the equivalence between the tracking error and identification error of unmodeled dynamics. This implies that the accurate tracking can be achieved by properly designing the hyper-parameters of ANNs. Besides, we also analyze and test the robustness of the controller against time delays and communication noise disturbances.

The remainder of this article is organized as follows. Section II briefly introduces MGs with a hierarchical control structure. Section III presents the model-free SVC along with the closed-loop stability analysis. Simulation results are presented in Section IV. Section V offers conclusions and future directions. All of the technical proofs are collected in the Appendix.

II. Problem Statement

A. Hierarchical Control of MGs

The hierarchical control structure is illustrated in Fig. 1. Primary control generally results in voltage deviations since it follows the droop control law. SVC is therefore used to compensate the deviations of voltage. In the islanded mode, the reference voltages, compactly denoted by $\boldsymbol{V}_o^{\text{ref}}$, are generally set as the nominal voltage of the MG, while in the grid-tied mode, they are determined by the tertiary control [3]. SVC generates control inputs $E_i^*, i = 1, \ldots, m$, according to the references and they are dispatched to each local primary controller of DERs. Then, the primary control calculates the voltage reference v_{oi}^* for the local inner control loops. Finally, the measured output voltages of DERs v_{oi} are measured and fed back to the SVC.

The secondary control has much slower dynamic response compared to primary control, which decouples the primary and secondary control [2]. This enables independent controller design at different layers. However, the flexibility of primary control is always limited to guarantee control performance when model-based control algorithms (e.g., feedback linearization and sliding mode control) are applied in the secondary layer. The a prior structures and parameters of primary control should be considered in SVC design and uncertainties and disturbances of primary layer could lead to instability and large tracking errors of MGs. This motivates us to develop a robust model-free SVC without knowing any specifications of primary layer.

B. Islanded MG System Description

In an islanded MG, the primary and inner control structures of inverter-based DERs are shown in Fig. 2. In the islanded mode, the control input of primary droop voltage controller is $E_i^*, \forall i$, which is obtained from SVC and the system output is the terminal voltage v_{oi}. Such MG system can be compactly expressed by a nonlinear state-space model as,

$$\dot{\boldsymbol{x}}(t) = f\big(\boldsymbol{x}(t), \boldsymbol{E}^*(t)\big) \tag{1a}$$

$$\boldsymbol{v}_o(t) = g(\boldsymbol{x}(t)) \tag{1b}$$

where $\boldsymbol{v}_o := [v_{o1}, \ldots, v_{om}]^T$; $\boldsymbol{x} := [\boldsymbol{x}_1^T, \ldots, \boldsymbol{x}_m^T]^T$; $\boldsymbol{E}^{*:=}[E_1^*, \ldots, E_m^*]^T$; $\boldsymbol{x}_i$ denotes the internal state variables of ith DER; f and g are the functions representing the nonlinear dynamic system.

Remark 1: Note that, Fig. 2 is only used to illustrate how the control signal E_i^* acts on the primary control layer, which is actually not needed for our SVC design benefiting from the model-free nature. In addition, this article focuses on SVC, so the design of frequency control is not limited, which also gives freedom to primary control, e.g., the PLL may not be needed when droop characteristics control the frequency [37]. Besides, functions f and g and state variables $\boldsymbol{x}$ are not necessarily required.

III. Model-Free SVC Based on Nonlinear Multiple Models Adaptive Control

In this section, a novel SVC method based on nonlinear multiple models adaptive control with unmodeled dynamics is proposed. We first present the design of linear and nonlinear controllers, respectively. Then, the controller parameter identification method is given. Finally, a switching mechanism is designed to coordinate the linear and nonlinear parts.

A. Optimal Controller Design for Voltage Regulation

Given that the measurements are sampled, system (1) are discretized as,

$$\boldsymbol{x}(k+1) = f\big(\boldsymbol{x}(k), \boldsymbol{E}^*(k)\big), \tag{2a}$$

$$\boldsymbol{v}_o(k) = g(\boldsymbol{x}(k)), \tag{2b}$$

where $\boldsymbol{E}^* \in \mathbb{R}^m, \boldsymbol{v}_o \in \mathbb{R}^m, \boldsymbol{x} \in \mathbb{R}^n$. The origin is an equilibrium of function f and g.

If system (2) is observable for nth order, the state variables of MGs $\boldsymbol{x}(k)$ can be expressed as a function of input and output variables, $\boldsymbol{v}_o(k), \ldots, \boldsymbol{v}_o(k-n+1), \boldsymbol{E}^*(k), \ldots, \boldsymbol{E}^*(k-n+1)$. Thus, (2) can be represented with only voltage control inputs and voltage outputs by the auto-regressive moving-average with exogenous input (ARMAX) model as,

$$\begin{aligned}\boldsymbol{A}\Big(z^{-1}\Big)\boldsymbol{v}_o(k+d) = \boldsymbol{B}\Big(z^{-1}\Big)\boldsymbol{E}^*(k) \\ + \boldsymbol{\varphi}[\boldsymbol{v}_o(k+d-1, \ldots, \boldsymbol{v}_o(k+d-n), \\ \boldsymbol{E}^*(k), \ldots, \boldsymbol{E}^*(k-n+1))\big],\end{aligned} \tag{3}$$

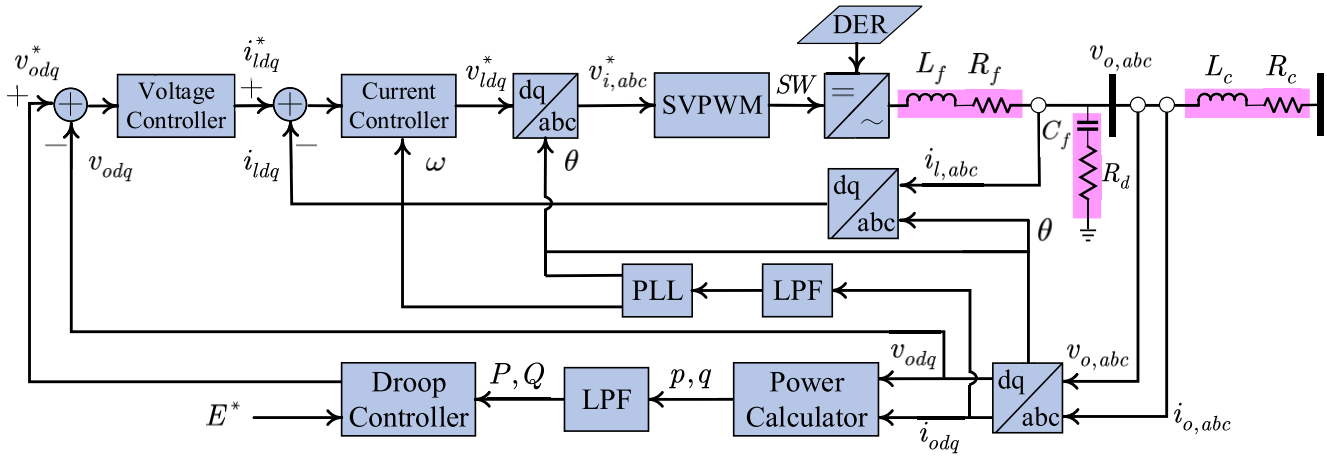

Fig. 2. The diagram of control structure of the VSC-based DER. PLL denotes the phase-locked loop; LPF denotes the low-pass filter; SVPWM denotes the space vector pulse width modulation.

where $\boldsymbol{A}(z^{-1})$ is an $m \times m$ matrix polynomial of nth-order backward shift operator; $\boldsymbol{B}(z^{-1})$ is an $m \times m$ matrix polynomial of $(n-1)$th-order backward shift operator; d $(1 \leq d \leq n)$ is the relative degree; $\boldsymbol{\varphi}[\,\cdot\,] \in \mathbb{R}^n$ is the unmodeled dynamics, which is a higher-order nonlinear function of $\boldsymbol{v}_o(k), \ldots, \boldsymbol{v}_o(k-n+1), \boldsymbol{E}^*(k), \ldots, \boldsymbol{E}^*(k-n+1)$ [38]. n and d are unknown if the detailed model of primary controllers and MGs are not available. However, they can be determined by the method in [39]. Moreover, the following assumptions are widely believed to hold for MGs in practice.

Assumption 1: (i) The internal dynamics of MGs are globally uniformly asymptotically stable; (ii) matrix polynomials $\boldsymbol{A}(z^{-1})$ and $\boldsymbol{B}(z^{-1})$ lie in a closed and bounded set Ω.

Assumption 1(i) ensures that the voltage control input $\boldsymbol{E}^*$ will not grow faster than the output voltage $\boldsymbol{v}_o$, indicating the MG is a minimum-phase system. Note that, this assumption is not necessary if the linear part of system (2) is asymptotically stable and thus, the proposed method can be applied to this kind of non-minimum-phase nonlinear system [40].

To ensure the stability while improving the voltage tracking performance, two separate optimal controllers are designed. We first define a cost function on voltage tracking errors,

$$J := \left\| \boldsymbol{F}\left(z^{-1}\right)\boldsymbol{v}_o(k+d) - \boldsymbol{R}\boldsymbol{v}_o^{\text{ref}}(k) \right\|^2, \tag{4}$$

where $\boldsymbol{v}_o^{\text{ref}} \in \mathbb{R}^m$ is voltage reference vector; $\boldsymbol{F}(\cdot)$ denotes an $m \times m$ weight matrix polynomial, which is stable and diagonal; $\boldsymbol{R}$ is an $m \times m$ diagonal real matrix.

To minimize (4), an optimal control law is designed as,

$$\boldsymbol{L}\left(z^{-1}\right)\boldsymbol{B}\left(z^{-1}\right)\boldsymbol{E}^*(k) + \boldsymbol{K}\left(z^{-1}\right)\boldsymbol{v}_o(k) + \boldsymbol{h}[\,\cdot\,] = \boldsymbol{R}\boldsymbol{v}_o^{\text{ref}}(k) \tag{5}$$

where $\boldsymbol{L}(z^{-1})$ denotes an $m \times m$ $(n-1)$th order polynomial, $\boldsymbol{K}(z^{-1}) := \boldsymbol{K}_0 + \boldsymbol{K}_1 z^{-1} + \cdots + \boldsymbol{K}_{n-1} z^{-n+1}$ is an $m \times m$ matrix polynomial and $\boldsymbol{h}[\,\cdot\,] := \boldsymbol{L}(z^{-1})\boldsymbol{\varphi}[\,\cdot\,]$. $\boldsymbol{L}(z^{-1})$ and $\boldsymbol{K}(z^{-1})$ can be calculated by,

$$\boldsymbol{F}\left(z^{-1}\right) = \boldsymbol{L}\left(z^{-1}\right)\boldsymbol{A}\left(z^{-1}\right) + z^{-d}\boldsymbol{K}\left(z^{-1}\right). \tag{6}$$

$\boldsymbol{h}[\cdot]$ in (5) is a linear transformation of unmodeled dynamics $\boldsymbol{\varphi}[\,\cdot\,]$, which can be estimated using ANNs. Let $\hat{\boldsymbol{h}}[\,\cdot\,]$ be its estimation, and then substitute (5) into (3), one can obtain,

$$\boldsymbol{F}\left(z^{-1}\right)\boldsymbol{v}_o(k+d) = \boldsymbol{R}\boldsymbol{v}_o^{\text{ref}}(k) + \boldsymbol{h}[\,\cdot\,] - \hat{\boldsymbol{h}}[\,\cdot\,] \tag{7}$$

where $\boldsymbol{F}(z^{-1})$ can be selected as a diagonal matrix such that its characteristic polynomial describes the poles of (7) and $\boldsymbol{R}$ can be chosen as $\boldsymbol{F}(1)$. If we obtain the linear parts of the system, the tracking error $\bar{\boldsymbol{e}} = \boldsymbol{F}(z^{-1})\boldsymbol{v}_o(k+d) - \boldsymbol{R}\boldsymbol{v}_o^{\text{ref}}(k)$ of the closed-loop system equals $\boldsymbol{h}[\,\cdot\,] - \hat{\boldsymbol{h}}[\,\cdot\,]$. With proper configuration of the ANNs, $\bar{\boldsymbol{e}}$ can be controlled to be arbitrarily small [38].

If the high-order nonlinear term $\boldsymbol{h}[\,\cdot\,]$ is small enough, (5) can be simplified as a linear control law as,

$$\boldsymbol{L}\left(z^{-1}\right)\boldsymbol{B}\left(z^{-1}\right)\boldsymbol{E}^*(k) + \boldsymbol{K}\left(z^{-1}\right)\boldsymbol{v}_o(k) = \boldsymbol{R}\boldsymbol{v}_o^{\text{ref}}(k). \tag{8}$$

B. Multiple Models Adaptive Control Based on ANNs

1) Identification of Controller Parameters: To achieve model-free control with *unknown* MG parameters, we propose to exploit the adaptive control method. From (3) and (6), we can obtain

$$\boldsymbol{y}(k+d) = \boldsymbol{\theta}^T\boldsymbol{\Psi}(k) + \boldsymbol{h}\left[\bar{\boldsymbol{\Psi}}(k)\right], \tag{9}$$

where $\boldsymbol{y}(k+d) := \boldsymbol{F}(z^{-1})\boldsymbol{v}_o(k+d)$ denotes the transformed output voltage; $\boldsymbol{\theta} := [\boldsymbol{K}_0, \ldots, \boldsymbol{K}_{n-1}, \boldsymbol{L}\boldsymbol{B}_0, \ldots, \boldsymbol{L}\boldsymbol{B}_{n+d-2}]^T$ denotes the input-output parameter matrix; $\boldsymbol{\Psi}(k) := [\boldsymbol{v}_o(k)^T, \ldots, \boldsymbol{v}_o(k-n+1)^T, \boldsymbol{E}^*(k)^T, \ldots, \boldsymbol{E}^*(k-n-d+2)^T]^T$ is the vector collecting all the output and input voltages, and $\bar{\boldsymbol{\Psi}}(k) = [\boldsymbol{v}_o(k), \ldots, \boldsymbol{v}_o(k-n+1), \boldsymbol{E}^*(k), \ldots, \boldsymbol{E}^*(k-n-d+2)]$. From Assumptions 1(ii), one can know that the parameter matrix $\boldsymbol{\theta}$ lies in a certain closed and bounded set. Assuming the unmodeled dynamics $\boldsymbol{h}[\,\cdot\,]$ are globally bounded by a known positive constant ρ, i.e., $\|\boldsymbol{h}[\,\cdot\,]\| \leq \rho$, we propose the linear and nonlinear model estimators for parameter identification. The linear estimator is designed as,

$$\hat{\boldsymbol{y}}_L(k+d) = \hat{\boldsymbol{\theta}}_L(k)^T\boldsymbol{\Psi}(k) \tag{10}$$

where $\hat{\boldsymbol{y}}_L$ and $\hat{\boldsymbol{\theta}}_L(k)$ are linear estimated transformed output voltage and linear estimated parameter vectors, respectively.

The update law is designed as,

$$\hat{\boldsymbol{\theta}}_L(k) = \text{proj}\left\{\hat{\boldsymbol{\theta}}'_L(k)\right\}, \tag{11}$$

$$\hat{\boldsymbol{\theta}}'_L(k) = \hat{\boldsymbol{\theta}}_L(k-d) + \frac{\eta_L(k)\boldsymbol{\Psi}(k-d)\boldsymbol{e}_L(k)^T}{1+\|\boldsymbol{\Psi}(k-d)\|^2}, \tag{12}$$

$$\eta_L(k) = \begin{cases} 1 & \text{if } \|\boldsymbol{e}_L(k)\| > 2\rho, \\ 0 & \text{otherwise,} \end{cases} \tag{13}$$

where $\boldsymbol{e}_L(k)$ is the identification error of linear model, i.e.,

$$\boldsymbol{e}_L(k) = \boldsymbol{y}(k) - \hat{\boldsymbol{\theta}}_L(k-d)^T\boldsymbol{\Psi}(k-d), \tag{14}$$

$\hat{\boldsymbol{\theta}}'_L(k) = [\hat{\boldsymbol{K}}_{1,0}(k), \ldots, \hat{\boldsymbol{K}}_{1,n-1}(k), \hat{\boldsymbol{L}}'_{1,0}(k)\ \hat{\boldsymbol{B}}'_{1,0}(k), \ldots, \hat{\boldsymbol{L}}_{1,n+d-2}(k)\ \hat{\boldsymbol{B}}_{1,n+d-2}(k)]^T$; proj$\{\cdot\}$ is a projection operator as

$$\text{proj}\{\hat{\boldsymbol{\theta}}'_L(k)\} = \begin{cases} \hat{\boldsymbol{\theta}}'_L(k) & \text{if } |\hat{\boldsymbol{L}}_{1,0}(k)\hat{\boldsymbol{B}}_{1,0}(k)| \geq h_{\min}, \\ [\cdots, h_{\min}, \ldots]^T & \text{otherwise,} \end{cases} \tag{15}$$

where $h_{\min} > 0$ is defined based on prior knowledge. This aims to prevent the control signal from being too big due to the too small identification parameter $\hat{\boldsymbol{L}}_{1,0}(k)\hat{\boldsymbol{B}}_{1,0}(k)$.

The nonlinear estimator is designed as,

$$\hat{\boldsymbol{y}}_N(k+d) = \hat{\boldsymbol{\theta}}_N(k)^T\boldsymbol{\Psi}(k) + \delta\hat{\boldsymbol{h}}\left[\bar{\boldsymbol{\Psi}}(k)\right], \tag{16}$$

where $\hat{\boldsymbol{y}}_N$ and $\hat{\boldsymbol{\theta}}_N$ are nonlinear estimated transformed output voltage and nonlinear estimated parameter vectors, respectively. $\delta\hat{\boldsymbol{h}}[\bar{\boldsymbol{\Psi}}(k)]$ is the estimation of $\delta\boldsymbol{h}[\bar{\boldsymbol{\Psi}}(k)]$ by ANNs at time instant k with $\delta\boldsymbol{h}[\bar{\boldsymbol{\Psi}}(k)] = \boldsymbol{y}(k+d) - \hat{\boldsymbol{\theta}}_N(k)^T\boldsymbol{\Psi}(k)$. According to [41], the only requirement on the update laws of $\hat{\boldsymbol{\theta}}_N(k)$ and $\hat{\boldsymbol{W}}(k)$ is that they always lie in certain compact set. Hence, the update law of $\hat{\boldsymbol{\theta}}_N(k)$ is designed similar to that of $\hat{\boldsymbol{\theta}}_L(k)$ where the difference is the definition of identification error, i.e.,

$$\boldsymbol{e}_N(k) = \boldsymbol{y}(k) - \hat{\boldsymbol{\theta}}_N(k-d)^T\boldsymbol{\Psi}(k-d) - \delta\hat{\boldsymbol{h}}\left[\bar{\boldsymbol{\Psi}}(k-d)\right]. \tag{17}$$

2) Nonlinear Identifier and Controller Based on ANNs: The voltage tracking performance of MGs heavily depends on the accuracy of estimation of the unmodeled dynamics, i.e., $\delta\boldsymbol{h}[\bar{\boldsymbol{\Psi}}(k)]$. As reported in [41], [42], ANNs are the universal approximators. Hence, by a proper choice of the structure and parameters of ANNs, the identification error of unmodeled dynamics $\|\delta\hat{\boldsymbol{h}} - \delta\boldsymbol{h}[\bar{\boldsymbol{\Psi}}(k)]\|$ can be made arbitrarily small over a compact set. We choose the back propagation (BP) ANN to estimate the unmodeled dynamics $\delta\boldsymbol{h}[\bar{\boldsymbol{\Psi}}(k)]$.

To guarantee that the hyper-parameters are well-tuned, we use the random search algorithm in [43] to calibrate the hyper-parameters based on the performance on a validation set. According to [38], with well-tuned hyper-parameters and appropriate training algorithm, one can obtain the estimation of ideal parameter matrix, $\hat{\boldsymbol{W}}(k)$ (containing weights and biases). Then, by taking $\hat{\boldsymbol{W}}(k)$ and $\boldsymbol{\Psi}(k)$ as the input vectors of the ANN function, it can achieve accurate and fast estimation of unmodeled dynamics. From a system theoretical point of view, ANNs are convenient families of nonlinear mappings as,

$$\begin{aligned}\delta\hat{\boldsymbol{h}}\left[\bar{\boldsymbol{\Psi}}(k)\right] &= \boldsymbol{\phi}\left[\hat{\boldsymbol{W}}(k), \boldsymbol{\Psi}(k)\right] \\ &= \hat{\boldsymbol{W}}_3(k)\boldsymbol{\Gamma}\left(\hat{\boldsymbol{W}}_2(k)\boldsymbol{\Gamma}\left(\hat{\boldsymbol{W}}_1(k)\boldsymbol{\Psi}(k) + \hat{\boldsymbol{b}}_1\right) + \hat{\boldsymbol{b}}_2\right) \\ &\quad + \hat{\boldsymbol{b}}_3\end{aligned} \tag{18}$$

where $\boldsymbol{\phi}[\cdot]$ represents the function of ANNs; $\hat{\boldsymbol{W}}_i$ and $\hat{\boldsymbol{b}}_i$ denote the ideal weight and bias vectors, respectively, $i = 1, 2, 3$; $\boldsymbol{\Gamma}$ represents a vector of activation functions.

3) Linear Adaptive Controller and ANN-Based Nonlinear Adaptive Controller: Finally, the linear adaptive controller (LAC) is designed as

$$\hat{\boldsymbol{\theta}}_L(k)^T\boldsymbol{\Psi}(k) = \boldsymbol{R}\boldsymbol{v}_o^{\text{ref}}(k). \tag{19}$$

Moreover, the nonlinear adaptive controller (NAC) based on ANN is designed as

$$\hat{\boldsymbol{\theta}}_N(k)^T\boldsymbol{\Psi}(k) + \delta\hat{\boldsymbol{h}}\left[\bar{\boldsymbol{\Psi}}(k)\right] = \boldsymbol{R}\boldsymbol{v}_o^{\text{ref}}(k). \tag{20}$$

4) Controller Design for Time Delays: In hierarchical control, the sampling time of SVC is larger than the primary control. The communication delays between the two levels can affect the stability and tracking performance of MGs. So, we consider a discrete-time system whose sampling time is equal to that of voltage measurement. We round the time delays to an integer multiple of the sampling period.

When there is no communication delay, i.e., $d = 1$, the predicted output $\hat{\boldsymbol{v}}_o(k)$ is computed with $\hat{\boldsymbol{\theta}}(k-1)$. However, when time delay exists, i.e., $d > 1$, the measured output voltage $\boldsymbol{v}_o(k)$ depends on the control input $\boldsymbol{E}^*(k-d)$ which is calculated with estimated parameters $\hat{\boldsymbol{\theta}}(k-d)$ using the then available measurement. Therefore, the identification error $\boldsymbol{e}(k)$ using $\hat{\boldsymbol{\theta}}(k-1)$ is equal to the tracking error $\bar{\boldsymbol{e}}(k)$ with delayed measurements. To solve this problem, the update law is designed in the form of (11)–(13). It can be elaborated that the sequence $\hat{\boldsymbol{\theta}}(k)$ are divided into d subsequences and each one updates itself when data is available. Note that, $\hat{\boldsymbol{W}}$ in (18) also needs to be split into d sequences and the corresponding ANNs update their parameters in their own time-scale.

C. Switching Mechanism

LAC aims to guarantee the stability while NAC is designed to achieve accurate voltage tracking. As shown in Fig. 3, the error between the weighted output voltage $\boldsymbol{F}\boldsymbol{v}_o$ of MGs and weighted desired voltage reference $\boldsymbol{R}\boldsymbol{v}_o^{\text{ref}}$ are given to the linear and nonlinear loops simultaneously at each time step k. In the nonlinear loop, NAC generates the voltage control signals $\boldsymbol{E}_{Ni}^*$ and transfers it to the nonlinear identified model based on ANNs. It is the same for the linear loop except that the controller and identifier are replaced by LAC and ARMAX model without ANN. Then, both linear and nonlinear identification errors, $\boldsymbol{e}_L$ and $\boldsymbol{e}_N$, are sent to the switching logic block. This block decides which controller is selected in the current time step. Finally, the selected voltage control signal is adopted in the primary control of DERs.

The performance index of switching mechanism is proposed based on a similar logic in [41]:

$$\begin{aligned}\xi_j(k) = &\sum_{s=d}^{k} \frac{\eta_j(s)\left(\|\boldsymbol{e}_j(s)\|^2 - 4\rho^2\right)}{2\left(1+\|\boldsymbol{\Psi}(s-d)\|^2\right)} \\ &+ \mu \sum_{s=k-M+1}^{k} \left(1-\eta_j(s)\right)\|\boldsymbol{e}_j(s)\|^2\end{aligned} \tag{21}$$

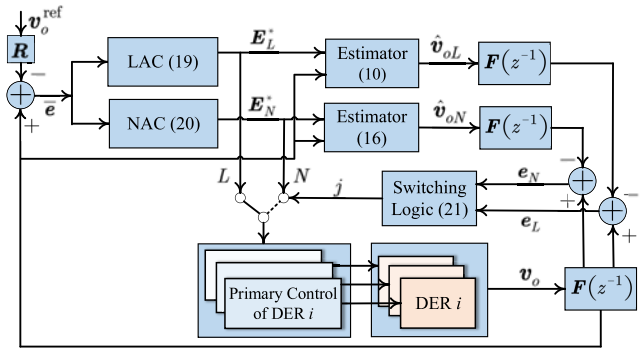

Fig. 3. The diagram of closed-loop MG system with proposed SVC using nonlinear multiple models adaptive control. When j switches to 'L', the linear estimator and controller are used; otherwise, the nonlinear ones are selected.

$$\eta_j(k) = \begin{cases} 1 & \text{if } \left\|\boldsymbol{e}_j(s)\right\| > 2\rho, \\ 0 & \text{otherwise,} \end{cases} \tag{22}$$

where $\mu \geq 0$ is a constant and M is a positive integer. We select the linear or nonlinear controller according to the smaller performance index:

$$\xi_* = \min[\xi_L, \xi_N]. \tag{23}$$

Note that, the performance index (21) is comprised of two terms. The first term is designed to differentiate signals with different rates to guarantee the boundedness of all signals, thus realizing stable switching. The second term is a measure of estimation errors over a period and is used to improve control performance [41]. When the linear or nonlinear identifier predicts the voltage with smaller errors, the second term decreases, thus the corresponding controller will be chosen. Properly selecting μ and M can enhance the stability. An outstanding advantage of such switching mechanism is that the stability and tracking performance can be decoupled. This means the hyper-parameters and training method of ANNs do not affect the stability.

When the ANN is degraded or disturbed, $\boldsymbol{e}_N$ increases. Consequently, $\xi_L < \xi_N$ and LAC is chosen. LAC keeps working to guarantee the stability until the ANN-based controller recovers. As $\boldsymbol{e}_N$ decreases, ξ_L is greater than ξ_N and the controller NAC is chosen to improve the performance. A proper selection of μ and ρ can enhance the voltage tracking performance while guaranteeing closed-loop stability.

Remark 3: According to the switched systems theory [44], it is possible to guarantee the stability with better performance by frequently switching controllers for unstable subsystems. However, such frequent switching may deteriorate the control performance or even cause instability in subsystems. Therefore, designing an appropriate switching mechanism is essential [45]. Our switching mechanism considers both the stability and voltage tracking performance.

D. Analysis of Stability and Tracking Error Convergence

In this section, we analyze the stability and voltage tracking errors of the closed-loop MG system with the proposed SVC method, which are detailed by the following propositions.

Proposition 1 (BIBO-Stability): For the system (3) with the control algorithm (10)–(22), suppose Assumption 1 holds and $\|\boldsymbol{h}[\cdot]\| \leq \rho$, the inputs $\boldsymbol{E}^*$ and output voltages $\boldsymbol{v}_o$ of MGs are uniformly bounded, i.e.,

$$\max_{0\leq\tau\leq k}\left\{\|\boldsymbol{v}_o(\tau)\|, \left\|\boldsymbol{E}^*(\tau)\right\|\right\} \leq \Delta \tag{24}$$

which holds for some positive constant Δ.

There are many kinds of stability definitions, such as Lyapunov stability, asymptotic stability, etc. For MG system which is nonlinear, these stability definitions only require the voltages converge to the stable operation point without boundedness. However, in practical operation, it is more important to ensure the voltage not to exceed the stability bound rather than to converge in infinite time. Therefore, in this article, we define the stability in a BIBO manner, which guarantees that all the output voltages of MGs are bounded. It is worth noting that our proposed control strategy naturally guarantees the inputs are bounded, which implies our method is much feasible in practice.

Proposition 2 (Tracking Error Convergence): With proper hyper-parameter calibration of ANNs and the proposed adaptive control method, the voltage tracking errors asymptotically converge to an arbitrarily small positive constant ϵ, i.e.,

$$\lim_{k\to\infty}\|\bar{\boldsymbol{e}}(k)\| = \lim_{k\to\infty}\left\|\boldsymbol{F}\left(z^{-1}\right)\boldsymbol{v}_o(k) - \boldsymbol{R}\boldsymbol{v}_o^{\text{ref}}(k-d)\right\| < \epsilon.$$

The proofs can be found in the Appendix.

Algorithm 1 Model-Free SVC

1: Measure the MG output voltage $\boldsymbol{v}_o(k)$ and establish data vector $\boldsymbol{\Psi}(k-d)$ together with SVC input $\boldsymbol{E}^*(k)$ at current time step.
2: **procedure** CONTROLLER SELECTION
3: Calculate the identification errors $\boldsymbol{e}_L(k)$ and $\boldsymbol{e}_N(k)$ using (14) and (17), respectively.
4: Calculate $\xi_L(k)$ and $\xi_N(k)$ with (21) and (22).
5: **if** $\xi_L(k) \leqslant \xi_N(k)$ **then**
6: j switches to position L and select linear controller
7: **else**
8: Let $j = N$ and select nonlinear controller.
9: **end if**
10: **end procedure**
11: **procedure** CONTROLLER CALCULATION
12: **if** $j = L$ **then**
13: Estimate LAC parameters $\hat{\boldsymbol{\theta}}_L(k)$ with (11)–(15), and calculate the SVC input $\boldsymbol{E}^*(k)$ using (19).
14: **else**
15: Estimate NAC parameters $\hat{\boldsymbol{\theta}}_L(k)$ with (17)–(18) and calculate $\boldsymbol{E}^*(k)$ using (20).
16: **end if**
17: **end procedure**
18: Let $k = k+1$, and return to Step 1.

E. Algorithm Implementation

The overall SVC algorithm design is presented in Algorithm 1. Firstly, $\boldsymbol{v}_o(k)$ is measured and sent to the SVC controller. The sampling rate of secondary control can be chosen from 100 Hz to 1 kHz [46]. Combining $\boldsymbol{v}_o(k)$ and $\boldsymbol{E}^*(k)$ with the historical data, we construct the data vector $\boldsymbol{\Psi}(k-d)$. The number of historical data depends on the n and d, which can be identified using the method in [39]. Then, the linear and nonlinear identifiers and controllers are established in the control center. The parameters ρ and μ in (21)–(23) can affect the

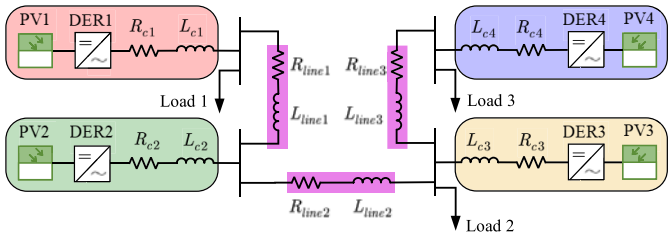

Fig. 4. MG test system.

TABLE I
PI PARAMETERS OF DERS

Controller	Parameter	Value	Parameter	Value
Voltage Controller	K_{PV1}	0.5	K_{IV1}	52
	K_{PV2}	0.5	K_{IV2}	52
	K_{PV3}	0.25	K_{IV3}	34
	K_{PV4}	0.25	K_{IV4}	34
Current Controller	K_{PC1}	4.5	K_{IC1}	450
	K_{PC2}	4.5	K_{IC2}	450
	K_{PC3}	3.55	K_{IC3}	353
	K_{PC4}	3.55	K_{IC4}	353

TABLE II
MG PARAMETERS

Parameter	Value	Parameter	Value
$L_{\mathrm{f1}}, L_{\mathrm{f2}}$	3.9 mH	$L_{\mathrm{f3}}, L_{\mathrm{f4}}$	3.9 mH
$R_{\mathrm{f1}}, R_{\mathrm{f2}}$	0.50 Ω	$R_{\mathrm{f3}}, R_{\mathrm{f4}}$	0.50 Ω
$L_{\mathrm{c1}}, L_{\mathrm{c2}}$	0.35 mH	$L_{\mathrm{c3}}, L_{\mathrm{c4}}$	0.45 mH
$R_{\mathrm{c1}}, R_{\mathrm{c2}}$	0.08 Ω	$R_{\mathrm{c3}}, R_{\mathrm{c4}}$	0.09 Ω
$C_{\mathrm{f1}}, C_{\mathrm{f2}}$	16 μF	$C_{\mathrm{f3}}, C_{\mathrm{f4}}$	16 μF
$R_{\mathrm{d1}}, R_{\mathrm{d2}}$	2.05 Ω	$R_{\mathrm{d3}}, R_{\mathrm{d4}}$	2.05 Ω
D_{Q1}	1×10^{-3} V/Var	D_{Q2}	1×10^{-3} V/Var
D_{Q3}	1.5×10^{-3} V/Var	D_{Q4}	1.5×10^{-3} V/Var
R_{line1}	0.15 Ω	L_{line1}	0.42 mH
R_{line2}	0.35 Ω	L_{line2}	0.33 mH
R_{line3}	0.23 Ω	L_{line3}	0.55 mH
P_{load1}	20 kW	Q_{load1}	9 kVar
P_{load2}	16 kW	Q_{load2}	9 kVar
P_{load3}	12 kW	Q_{load3}	6 kVar

tracking performance. As ρ decreases, the accuracy of linear parts increases. But if ρ is too small, the parameter updating process converges slowly. μ represents the weight of tracking performance. To balance the stability and control performance, μ is usually selected around 1.5 [38]. The widely-used two-way communication network between MGCC and DERs is required [47].

IV. CASE STUDIES

A. Simulation Setup

The proposed SVC is tested on a widely used MG system (see Fig. 4), originally consisting of four inverter-based DERs and two loads [48]. The control system of DERs has been shown in Fig. 2. The MG parameters are given in Table II. The sampling periods of primary and secondary control are set as 10^{-4} s and 0.01 s, respectively. The total simulation time is 10 s. All the dynamic simulations are implemented in MATLAB/Simulink environment.

We establish a feed-forward ANN consisting of two hidden layers (50 and 8 nodes, respectively). To obtain the training set, we first only adopt the LAC and make $\boldsymbol{v}_o^{\mathrm{ref}}$ time-varying instead of a constant. When finishing this case, we select the current and historical control inputs $\boldsymbol{E}^*(k), \ldots, \boldsymbol{E}^*(k-n+1)$, $k = 1, \ldots, 1000$ and output voltages $\boldsymbol{v}_o(k+d-1), \ldots, \boldsymbol{v}_o(k+d-n)$ as the inputs of the training of ANN. While the errors between the output voltage of the linear model with LAC and real voltages $h(\bar{\boldsymbol{\Psi}}(k)) = \boldsymbol{v}_o(k+d) - \hat{\boldsymbol{v}}_o(k+d) = \boldsymbol{y}(k) - \hat{\boldsymbol{\theta}}_L(k)^T \boldsymbol{\Psi}(k)$ are used as the output of the training set. The ANN is trained offline using back-propagation with Levenberg-Marquardt algorithm [49]. The learning rate is set as $lr = 0.9$, and the momentum factor is selected as $mc = 0.8$. The activation function for the first and second hidden layers are selected as "tansig" and "purelin", respectively. The offline training of ANN takes 29.36 s and 1675 iterations. The mean squared error of training and test are 9.94×10^{-6} and 3.85×10^{-3}, respectively. The trained ANN is integrated into the NAC as an identifier.

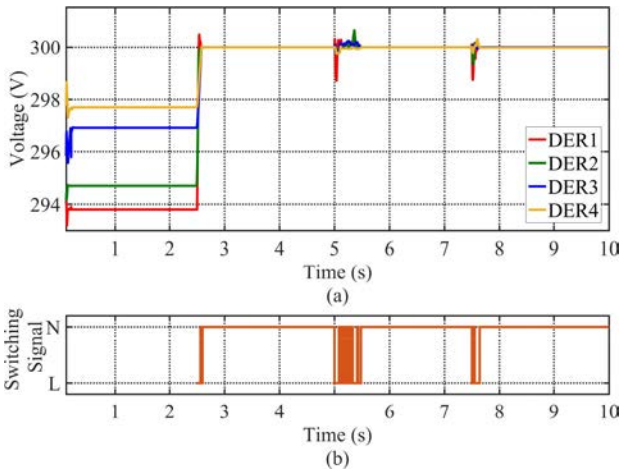

Fig. 5. Voltage tracking performance of the proposed controller.

B. Tracking Performance

The voltage tracking performance is shown in Fig. 5. The reference voltages are set as 300 V. The SVC is not applied until $t = 2.5$ s. Before that though voltages are stable, steady state errors still exist. Once SVC is implemented, the voltage magnitudes are restored to the reference values rapidly. At $t = 5$ s, a constant power load is attached to the system. To show the robustness of the model-free method, a parameter perturbation that L_{c1} is reduced by 25% is triggered since $t = 7.5$ s. From Fig. 5(b), we notice that when large disturbances happen, the control mode oscillates between the LAC and NAC due to the degradation of ANNs. The switching mechanism is trying to balance the tracking performance and stability. Once ANN recovers, it switches back to NAC. The results show that the proposed SVC exhibits good voltage tracking performance and robustness to the uncertain perturbations. Fig. 6 shows that the active power outputs of DERs are allocated according to their rated power.

C. Stability of LAC

One may doubt that what if the ANN is not well-trained or its hyper-parameters are not well-tuned. To verify the stabilization of the proposed controller, we only use the LAC by

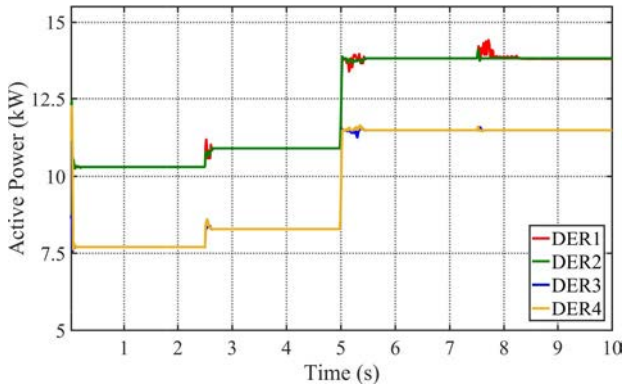

Fig. 6. Active power outputs using multiple models adaptive control.

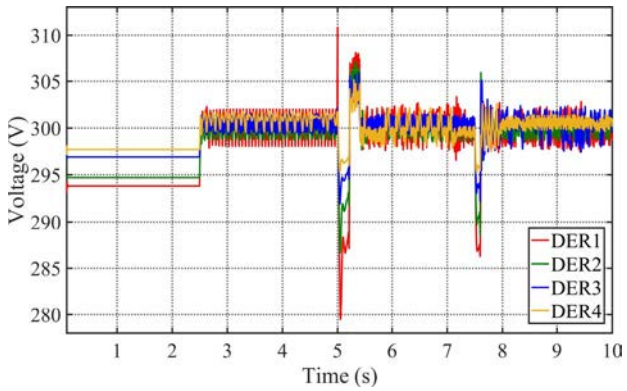

Fig. 7. Stability performance of voltage using LAC.

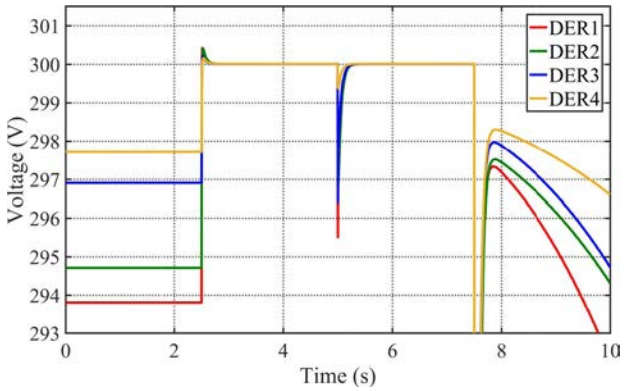

Fig. 8. Voltage tracking performance of feedback linearization control.

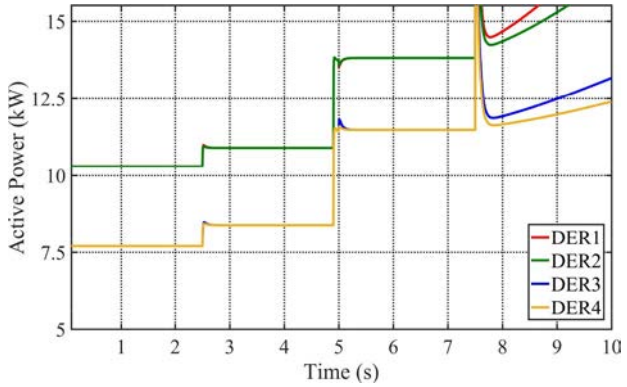

Fig. 9. Active power outputs of DERs with feedback linearization control.

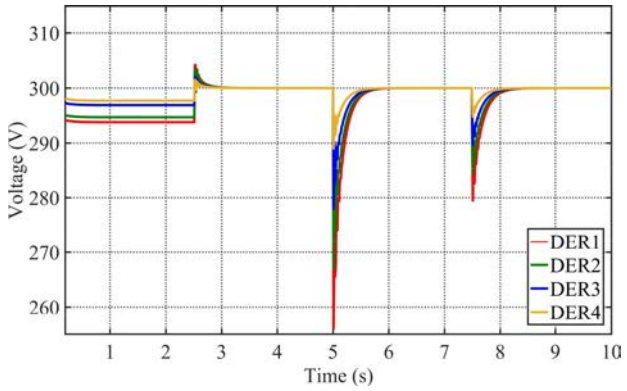

Fig. 10. Voltage tracking performance of PID control.

fixing $j \leftarrow L$. The results are shown in Fig. 7. Due to the inaccuracy of linearized model, the parameters are kept updating automatically, which leads to the oscillations of output voltages. However, the stability is still guaranteed and the errors between real and reference voltages are maintained bounded, even when large disturbances occur.

D. Comparison With Feedback Linearization Control

A comparison study with input-output feedback linearization control, which is well-known as nonlinear control method requiring precise model, is carried out in this section. When load 3 is attached at $t = 5$ s, we assume the information of load change is known by the secondary controller based on feedback linearization. Similarly, an unknown parameter perturbation occurs at $t = 7.5$ s. As shown in Fig. 8, though the feedback linearization controller can deal with the *known* large load fluctuation, it fails to restore and stabilize the output voltages in case of *uncertainties*. The corresponding active power outputs are shown in Fig. 9.

E. Comparison With PID Control

To compare the proposed method with the existing model-free approaches, in this section, we conduct simulations by the most widely-used model-free PID control. Fig. 10 and Fig. 11 show that, under the same conditions, the PID control can realize accurate voltage tracking and is robust to unknown parameter perturbation. However, compared with the proposed method, PID control performs more sluggish transient responses and much larger overshootings after large load disturbance and parameter perturbation.

F. Effect of Time Delays

In this section, we test the robustness of the proposed controller against time delays. The sampling time $\Delta T = 10$ ms. We set the time delays as $\{(d-1) \times \Delta T | d = 1, 2, 3, 5, 10, 20\}$, respectively. Any fractional time delays are rounded up. Load 3 is attached at $t = 5$ s. Fig. 12 shows the comparison of voltage tracking performances with different time delays of DER1. The blue line shows the result without time delay, i.e., $d = 1$. The red line shows the worst case with a delay of 190 ms. The result shows that the proposed controller can stabilize the system with any different delays. However,

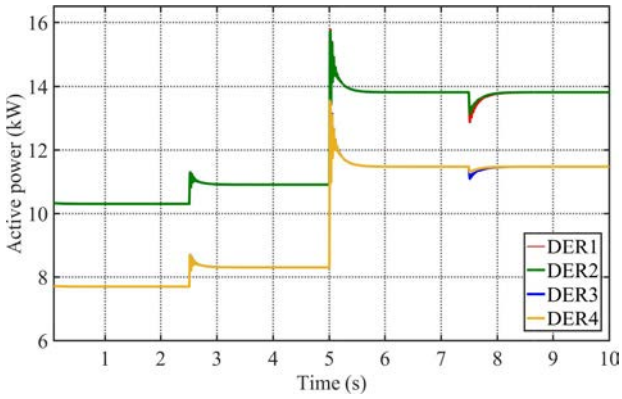

Fig. 11. Active power outputs of DERs with PID control.

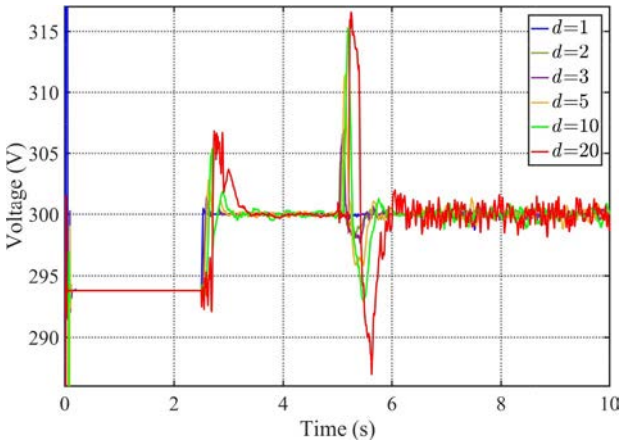

Fig. 12. Voltage tracking performance with different time delays; SVC is applied after 2.5 s; load 3 is attached at 5 s.

as time delay increases, the settling time and overshoot of transient responses become larger. For steady-state operation, there are larger oscillations under larger time delays.

G. Effect of Communication Noise Disturbances

The noise disturbances in communication links between secondary and primary levels widely exist in the SVC of MGs and may degrade the dynamic performance of the controller. To study the influence of communication noise disturbances on the proposed SVC method, white noises with signal-to-noise ratio (SNR) of 30 dB, 20 dB and 10 dB are added to the communication links between SVC and primary level. Note that smaller SNR indicates larger noise disturbance, and the SNR is usually between 30 to 40 dB in MGs [50], [51]. As shown in Fig. 13, the proposed SVC method can realize voltage tracking and BIBO stability with some ripples under small communication noise disturbances; however, the dynamic performance degrades when noise enlarges.

V. Conclusion

In this article, we proposed a novel model-free SVC using nonlinear multiple models adaptive control. The MGs with primary control are treated as a "black-box" when designing the SVC. The proposed controller consists of two separate parts, i.e., LAC and NAC, which are coordinated by a switching mechanism. The unmodeled nonlinear dynamics are online

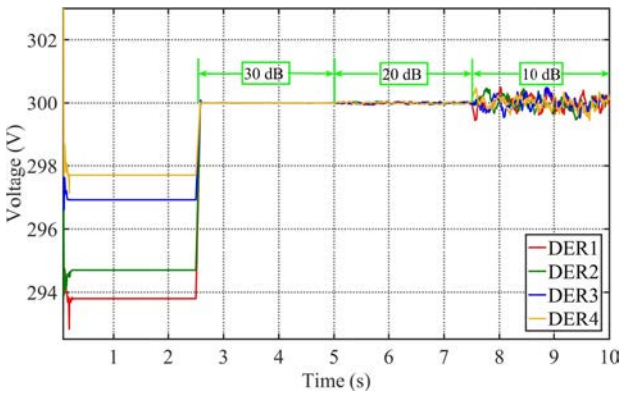

Fig. 13. Voltage tracking performance with different communication noise disturbances. Communication noises with 30 dB, 20 dB and 10 dB SNR are added at 2.5 s, 5 s, and 7.5 s, respectively.

estimated by ANNs. We have proved that the tracking errors can be achieved arbitrarily small given a proper nonlinear identification. The simulation results show that such switching mechanism can guarantee BIBO stability of the closed-loop system while achieving accurate tracking. The proposed controller is robust to uncertainties, disturbances and time delays.

Due to the advantages of flexibility and robustness, the distributed and decentralized model-free secondary voltage control will be further investigated in our future works.

Appendix

Proof of Proposition 1: This proof can be separated into two parts: the BIBO stability of output voltage and the convergence of voltage tracking error. For the proof of stability, we first prove that SVC input $\boldsymbol{E}^*$ and output voltage $\boldsymbol{v}_o$ are bounded by $\boldsymbol{e}$, then we use the contradiction argument to prove that $\boldsymbol{e}$ is bounded, and that means $\boldsymbol{E}^*$ and $\boldsymbol{v}_o$ are also bounded.

Define the parameter identification error of linear estimator as $\boldsymbol{\psi}_L(k) = \hat{\boldsymbol{\theta}}_L(k) - \boldsymbol{\theta}$. By (12), it follows that

$$\boldsymbol{\psi}_L(k) = \boldsymbol{\psi}_L(k-d) + \frac{\eta_L(k)\boldsymbol{\Psi}(k-d)\boldsymbol{e}_L(k)^T}{1+\|\boldsymbol{\Psi}(k-d)\|^2}. \tag{25}$$

Following the proof in [41] and from the logic function (22), it can be proven that $\hat{\boldsymbol{\theta}}_L(k)$ is bounded. In addition,

$$\lim_{N\to\infty}\sum_{k=d}^{N}\frac{\eta_L(k)\big(\|\boldsymbol{e}_L(k)\|^2-4\rho^2\big)}{2\big(1+\|\boldsymbol{\Psi}(k-d)\|^2\big)} < \infty, \tag{26}$$

$$\lim_{k\to\infty}\frac{\eta_L(k)\big(\|\boldsymbol{e}_L(k)\|^2-4\rho^2\big)}{2\big(1+\|\boldsymbol{\Psi}(k-d)\|^2\big)} \to 0. \tag{27}$$

From (14) and (19), we have

$$\boldsymbol{e}_L(k) = \boldsymbol{F}\left(z^{-1}\right)\boldsymbol{v}_o(k) - \boldsymbol{R}\boldsymbol{v}_o^{\text{ref}}(k-d). \tag{28}$$

Since $\boldsymbol{F}(z^{-1})$ is stable, then from (28), there exist positive constants ℓ_1 and ℓ_2 such that

$$\|\boldsymbol{\Psi}(k-d)\| \le \ell_1 + \ell_2 \max_{0\le\tau\le k}\|\boldsymbol{e}_L(\tau)\|. \tag{29}$$

which indicates that the input $\boldsymbol{E}^*$ and output voltage $\boldsymbol{v}_o$ are bounded by the linear identification error $\boldsymbol{e}_L$.

To prove the boundedness of $\boldsymbol{e}_L$, we utilize the proof by contradiction argument. Suppose that $\boldsymbol{e}_L(k)$ is unbounded, then

there must exist a positive time constant T, such that $\|\boldsymbol{e}_L(k)\| > 2\rho$ and $a_L(k) = 1$ for $k > T$, i.e., there exists a monotonic increasing sequence $\|\boldsymbol{e}_L(k_n)\|$ such that $\lim_{k_n\to\infty}\|\boldsymbol{e}_L(k_n)\| = \infty$. Then, it follows that

$$\begin{aligned}
&\lim_{k_n\to\infty}\frac{\eta_L(k_n)\big(\|\boldsymbol{e}_L(k_n)\|^2-4\rho^2\big)}{2\big(1+\|\boldsymbol{\Psi}(k_n-d)\|^2\big)}\\
&\geq \lim_{k_n\to\infty}\frac{\eta_L(k_n)\big(\|\boldsymbol{e}_L(k_n)\|^2-4\rho^2\big)}{2\Big(1+\big(\ell_1+\ell_2\max_{0\leq\tau\leq k}\|\boldsymbol{e}_L(\tau)\|\big)^2\Big)}\\
&\geq \lim_{k_n\to\infty}\frac{\eta_L(k_n)\big(\|\boldsymbol{e}_L(k_n)\|^2-4\rho^2\big)}{2\big(1+(\ell_1+\ell_2\|\boldsymbol{e}_L(k_n)\|)^2\big)}\\
&\geq \frac{1}{2\ell_2^2}\\
&> 0.
\end{aligned}\tag{30}$$

However, it contradicts (27) which means $\boldsymbol{e}_L(k)$ is bounded. Thus, it proves the BIBO stability for LAC. For NAC, from (17) and (20), it follows that,

$$\boldsymbol{e}_N(k) = \boldsymbol{F}\Big(z^{-1}\Big)\boldsymbol{v}_o(k) - \boldsymbol{R}\boldsymbol{v}_o^{\text{ref}}(k-d).\tag{31}$$

Since $\boldsymbol{F}(z^{-1})$ is stable, then from (31), there exist positive constants ℓ_3 and ℓ_4 such that

$$\|\boldsymbol{\Psi}(k-d)\| \leq \ell_3 + \ell_4\max_{0\leq\tau\leq k}\|\boldsymbol{e}_N(\tau)\|.\tag{32}$$

The first term in (21) is bounded according to (26), and the second term is also bounded due to the dead-zone function (22). Hence $\xi_L(k)$ is bounded. If $\xi_N(k)$ is bounded, according to the switching mechanism function (21), we have

$$\lim_{k\to\infty}\frac{\eta_N(k)\big(\|\boldsymbol{e}_N(k)\|^2-4\rho^2\big)}{2\big(1+\|\boldsymbol{\Psi}(k-d)\|^2\big)}\to 0.\tag{33}$$

In this case, both of linear of nonlinear identification errors of the closed-loop MG system $\boldsymbol{e}_j(k)$, $j=\{L,N\}$ satisfy that

$$\lim_{k\to\infty}\frac{\eta(k)\big(\|\boldsymbol{e}(k)\|^2-4\rho^2\big)}{2\big(1+\|\boldsymbol{\Psi}(k-d)\|^2\big)}\to 0,\tag{34}$$

where

$$a(k) = \begin{cases}1, & \text{if } \|\boldsymbol{e}(k)\| > 2\rho,\\ 0, & \text{otherwise.}\end{cases}\tag{35}$$

If $\xi_N(k)$ is unbounded, considering $\xi_L(k)$ is bounded, there must exist $k_0 > 0$ such that $\xi_L(k) \leq \xi_N(k)$, $\forall k \geq k_0$. Then after time k_0, the switching mechanism will choose the linear controller, thus the identification error $\boldsymbol{e}(k) = \boldsymbol{e}_L(k)$ which also satisfies (34).

Finally, from (29), (32) and (34), it can be proved that $\boldsymbol{v}_o$ and $\boldsymbol{E}^*$ are bounded, i.e., the input and output of the closed-loop switching system are bounded while the identification error $\boldsymbol{e}_j(k)$ satisfies

$$\lim_{k\to\infty}\big\|\boldsymbol{e}_j(k)\big\| \leq 2\rho,\quad j=\{L,N\}\tag{36}$$

which indicates that there exist positive constants ℓ_5 and ℓ_6 such that,

$$\|\boldsymbol{\Psi}(k-d)\| \leq \ell_5 + \ell_6\max_{0\leq\tau\leq k}\big\|\boldsymbol{e}_j(\tau)\big\| \leq \ell_5 + 2\ell_6\rho.\tag{37}$$

Let $\Delta = \ell_5 + 2\ell_6\rho$, it follows that

$$\max_{0\leq\tau\leq k}\big\{\|\boldsymbol{v}_o(\tau)\|, \big\|\boldsymbol{E}^*(\tau)\big\|\big\} \leq \Delta.\tag{38}$$

Now we have proven the BIBO voltage stability of the closed-loop MG system with the proposed SVC.

Proof of Proposition 2: Switching mechanism always selects the controller, with respect to the smaller identification error, as the SVC input for MG system. Moreover, from (28) and (31), the output voltage tracking error $\bar{\boldsymbol{e}}(k)$ is equivalent to the smaller identification error. From (17), we have the nonlinear identification error,

$$\begin{aligned}
\boldsymbol{e}_N(k) &= \boldsymbol{y}_N(k) - \hat{\boldsymbol{\theta}}_N(k-d)^T\boldsymbol{\Psi}(k-d) - \delta\hat{\boldsymbol{h}}\big[\bar{\boldsymbol{\Psi}}(k-d)\big]\\
&= \boldsymbol{y}_N(k) - \big(\boldsymbol{y}_N(k) - \delta\boldsymbol{h}\big[\bar{\boldsymbol{\Psi}}(k-d)\big]\big) - \delta\hat{\boldsymbol{h}}\big[\bar{\boldsymbol{\Psi}}(k-d)\big]\\
&= \delta\boldsymbol{h}\big[\bar{\boldsymbol{\Psi}}(k-d)\big] - \delta\hat{\boldsymbol{h}}\big[\bar{\boldsymbol{\Psi}}(k-d)\big].
\end{aligned}\tag{39}$$

When the hyper-parameters of the ANN are well-tuned, for arbitrary small positive constant ϵ, the voltage tracking error always satisfies $\|\delta\boldsymbol{h}[\bar{\boldsymbol{\Psi}}(k-d)] - \delta\hat{\boldsymbol{h}}[\bar{\boldsymbol{\Psi}}(k-d)]\| < \epsilon$. It means the nonlinear identification error is always smaller than the linear one, so that the tracking error will be automatically selected as the nonlinear identification error, i.e.,

$$\lim_{k\to\infty}\|\bar{\boldsymbol{e}}(k)\| = \lim_{k\to\infty}\|\boldsymbol{e}_N(k)\| < \epsilon.\tag{40}$$

REFERENCES

[1] J. C. Vasquez, J. M. Guerrero, J. Miret, M. Castilla, and L. G. de Vicuña, "Hierarchical control of intelligent microgrids," *IEEE Ind. Electron. Mag.*, vol. 4, no. 4, pp. 23–29, Dec. 2010.

[2] J. M. Guerrero, J. C. Vasquez, J. Matas, L. G. De Vicuña, and M. Castilla, "Hierarchical control of droop-controlled AC and DC microgrids—A general approach toward standardization," *IEEE Trans. Ind. Electron.*, vol. 58, no. 1, pp. 158–172, Jan. 2011.

[3] A. Bidram and A. Davoudi, "Hierarchical structure of microgrids control system," *IEEE Trans. Smart Grid*, vol. 3, no. 4, pp. 1963–1976, Dec. 2012.

[4] N. Jumpasri, K. Pinsuntia, K. Woranetsuttikul, T. Nilsakorn, and W. Khan-ngern, "Comparison of distributed and centralized control for partial shading in PV parallel based on particle swarm optimization algorithm," in *Proc. Int. Elect. Eng. Congr. (iEECON)*, Chonburi, Thailand, 2014, pp. 1–4.

[5] T. Morstyn, B. Hredzak, and V. G. Agelidis, "Distributed cooperative control of microgrid storage," *IEEE Trans. Power Syst.*, vol. 30, no. 5, pp. 2780–2789, Sep. 2015.

[6] T. Dragicevic, X. Lu, J. C. Vasquez, and J. M. Guerrero, "DC microgrids—Part I: A review of control strategies and stabilization techniques," *IEEE Trans. Power Electron.*, vol. 31, no. 7, pp. 4876–4891, Jul. 2016.

[7] Q. Shafiee, J. M. Guerrero, and J. C. Vasquez, "Distributed secondary control for islanded microgrids—A novel approach," *IEEE Trans. Power Electron.*, vol. 29, no. 2, pp. 1018–1031, Feb. 2014.

[8] J. W. Simpson-Porco, F. Dörfler, and F. Bullo, "Synchronization and power sharing for droop-controlled inverters in islanded microgrids," *Automatica*, vol. 49, no. 9, pp. 2603–2611, Dec. 2013.

[9] B. Wei, Y. Gui, S. Trujillo, J. M. Guerrero, J. C. Vásquez, and A. Marzábal, "Distributed average integral secondary control for modular ups systems-based microgrids," *IEEE Trans. Power Electron.*, vol. 34, no. 7, pp. 6922–6936, Jul. 2019.

[10] Q. Shafiee, Č. Stefanović, T. Dragičević, P. Popovski, J. C. Vasquez, and J. M. Guerrero, "Robust networked control scheme for distributed secondary control of islanded microgrids," *IEEE Trans. Ind. Electron.*, vol. 61, no. 10, pp. 5363–5374, Oct. 2014.

[11] A. Bidram, A. Davoudi, F. L. Lewis, and Z. Qu, "Secondary control of microgrids based on distributed cooperative control of multi-agent systems," *IET Gener. Transm. Distrib.*, vol. 7, no. 8, pp. 822–831, Aug. 2013.

[12] A. Bidram, A. Davoudi, F. L. Lewis, and S. S. Ge, "Distributed adaptive voltage control of inverter-based microgrids," *IEEE Trans. Energy Convers.*, vol. 29, no. 4, pp. 862–872, Dec. 2014.
[13] Y. Guo, H. Gao, and Q. Wu, "Distributed cooperative voltage control of wind farms based on consensus protocol," *Int. J. Elect. Power Energy Syst.*, vol. 104, pp. 593–602, Jan. 2019.
[14] Z. Ma, Z. Wang, and Y. Yuan, Y. Wang, R. Diao, and D. Shi, "Stability and accuracy assessment based large-signal order reduction of microgrids," 2019. [Online]. Available: arXiv:1910.03687.
[15] A. Bidram, A. Davoudi, F. L. Lewis, and J. M. Guerrero, "Distributed cooperative secondary control of microgrids using feedback linearization," *IEEE Trans. Power Syst.*, vol. 28, no. 3, pp. 3462–3470, Aug. 2013.
[16] C. Ahumada, R. Cárdenas, D. Sáez, and J. M. Guerrero, "Secondary control strategies for frequency restoration in islanded microgrids with consideration of communication delays," *IEEE Trans. Smart Grid*, vol. 7, no. 3, pp. 1430–1441, May 2016.
[17] M. Mokhtar, M. I. Marei, and A. A. El-Sattar, "An adaptive droop control scheme for DC microgrids integrating sliding mode voltage and current controlled boost converters," *IEEE Trans. Smart Grid*, vol. 10, no. 2, pp. 1685–1693, Mar. 2019.
[18] C. Wang, P. Yang, C. Ye, Y. Wang, and Z. Xu, "Voltage control strategy for three/single phase hybrid multimicrogrid," *IEEE Trans. Energy Convers.*, vol. 31, no. 4, pp. 1498–1509, Dec. 2016.
[19] M. J. Hossain, M. A. Mahmud, F. Milano, S. Bacha, and A. Hably, "Design of robust distributed control for interconnected microgrids," *IEEE Trans. Smart Grid*, vol. 7, no. 6, pp. 2724–2735, Nov. 2016.
[20] F. Guo, C. Wen, J. Mao, and Y. Song, "Distributed secondary voltage and frequency restoration control of droop-controlled inverter-based microgrids," *IEEE Trans. Ind. Electron.*, vol. 62, no. 7, pp. 4355–4364, Jul. 2015.
[21] H. Cai, G. Hu, F. L. Lewis, and A. Davoudi, "A distributed feedforward approach to cooperative control of AC microgrids," *IEEE Trans. Power Syst.*, vol. 31, no. 5, pp. 4057–4067, Sep. 2016.
[22] N. M. Dehkordi, N. Sadati, and M. Hamzeh, "Distributed robust finite-time secondary voltage and frequency control of islanded microgrids," *IEEE Trans. Power Syst.*, vol. 32, no. 5, pp. 3648–3659, Sep. 2017.
[23] A. H. Etemadi, E. J. Davison, and R. Iravani, "A decentralized robust control strategy for multi-DER microgrids—Part I: Fundamental concepts," *IEEE Trans. Power Del.*, vol. 27, no. 4, pp. 1843–1853, Oct. 2012.
[24] T. Geyer and D. E. Quevedo, "Multistep finite control set model predictive control for power electronics," *IEEE Trans. Power Electron.*, vol. 29, no. 12, pp. 6836–6846, Dec. 2014.
[25] M. Davari and Y. A. I. Mohamed, "Variable-structure-based nonlinear control for the master VSC in DC-energy-pool multiterminal grids," *IEEE Trans. Power Electron.*, vol. 29, no. 11, pp. 6196–6213, Nov. 2014.
[26] J. Lai, X. Lu, and X. Yu, "Stochastic distributed frequency and load sharing control for microgrids with communication delays," *IEEE Syst. J.*, vol. 13, no. 4, pp. 4269–4280, Dec. 2019.
[27] J. Lai, X. Lu, X. Yu, and A. Monti, "Stochastic distributed secondary control for AC microgrids via event-triggered communication," *IEEE Trans. Smart Grid*, vol. 11, no. 4, pp. 2746–2759, Jul. 2020.
[28] M. Khooban, "Secondary load frequency control of time-delay standalone microgrids with electric vehicles," *IEEE Trans. Ind. Electron.*, vol. 65, no. 9, pp. 7416–7422, Sep. 2018.
[29] H. Zhang, J. Zhou, Q. Sun, J. M. Guerrero, and D. Ma, "Data-driven control for interlinked AC/DC microgrids via model-free adaptive control and dual-droop control," *IEEE Trans. Smart Grid*, vol. 8, no. 2, pp. 557–571, Mar. 2017.
[30] C. Ahn and H. Peng, "Decentralized voltage control to minimize distribution power loss of microgrids," *IEEE Trans. Smart Grid*, vol. 4, no. 3, pp. 1297–1304, Sep. 2013.
[31] M. Khooban *et al.*, "Robust frequency regulation in mobile microgrids: HIL implementation," *IEEE Syst. J.*, vol. 13, no. 4, pp. 4281–4291, Dec. 2019.
[32] V. Utkin, "Discussion aspects of high-order sliding mode control," *IEEE Trans. Autom. Control*, vol. 61, no. 3, pp. 829–833, Mar. 2016.
[33] J. W. Simpson-Porco, Q. Shafiee, F. Dörfler, J. C. Vasquez, J. M. Guerrero, and F. Bullo, "Secondary frequency and voltage control of islanded microgrids via distributed averaging," *IEEE Trans. Ind. Electron.*, vol. 62, no. 11, pp. 7025–7038, Nov. 2015.
[34] H. Zhang, C. Qin, B. Jiang, and Y. Luo, "Online adaptive policy learning algorithm for h_∞ state feedback control of unknown affine nonlinear discrete-time systems," *IEEE Trans. Cybern.*, vol. 44, no. 12, pp. 2706–2718, Dec. 2014.
[35] H. Zhang and Y. Quan, "Modeling, identification, and control of a class of nonlinear systems," *IEEE Trans. Fuzzy Syst.*, vol. 9, no. 2, pp. 349–354, Apr. 2001.
[36] T. Sreekumar and K. S. Jiji, "Comparison of proportional-integral (P-I) and integral-proportional (I-P) controllers for speed control in vector controlled induction motor drive," in *Proc. 2nd Int. Conf. Power Control Embedded Syst.*, Allahabad, India, Dec. 2012, pp. 1–6.
[37] N. Kroutikova, C. A. Hernandez-Aramburo, and T. C. Green, "State-space model of grid-connected inverters under current control mode," *IET Elect. Power Appl.*, vol. 1, no. 3, pp. 329–338, May 2007.
[38] Y. Fu and T. Chai, "Nonlinear multivariable adaptive control using multiple models and neural networks," *Automatica*, vol. 43, no. 6, pp. 1101–1110, Jun. 2007.
[39] D. Erdogmus, J. Cho, J. Lan, M. Motter, and J. C. Principe, "Adaptive local linear modelling and control of nonlinear dynamical systems," *IEE Control Eng. Series*, vol. 70, p. 119, Jul. 2005.
[40] Y. Zhang, T. Chai, H. Wang, J. Fu, L. Zhang, and Y. Wang, "An adaptive generalized predictive control method for nonlinear systems based on anfis and multiple models," *IEEE Trans. Fuzzy Syst.*, vol. 18, no. 6, pp. 1070–1082, Dec. 2010.
[41] L. Chen and K. S. Narendra, "Nonlinear adaptive control using neural networks and multiple models," *Automatica*, vol. 37, no. 8, pp. 1245–1255, Aug. 2001.
[42] K.-I. Funahashi, "On the approximate realization of continuous mappings by neural networks," *Neural Netw.*, vol. 2, no. 3, pp. 183–192, 1989.
[43] H. Larochelle, D. Erhan, A. Courville, J. Bergstra, and Y. Bengio, "An empirical evaluation of deep architectures on problems with many factors of variation," in *Proc. 24th Int. Conf. Mach. Learn.*, 2007, pp. 473–480.
[44] J. Li, Z. Ma, and J. Fu, "Exponential stabilization of switched discrete-time systems with all unstable modes," *Asian J. Control*, vol. 20, no. 1, pp. 608–612, Sep. 2018.
[45] J. Lai, X. Lu, X. Yu, A. Monti, and H. Zhou, "Distributed voltage regulation for cyber-physical microgrids with coupling delays and slow switching topologies," *IEEE Trans. Syst., Man, Cybern., Syst*, vol. 50, no. 1, pp. 100–110, Jan. 2020.
[46] C. Zhao, W. Sun, J. Wang, Q. Li, D. Mu, and X. Xu, "Distributed cooperative secondary control for islanded microgrid with Markov time-varying delays," *IEEE Trans. Energy Convers.*, vol. 34, no. 4, pp. 2235–2247, Dec. 2019.
[47] A. C. Z. de Souza and M. Castilla, *Microgrids Design and Implementation*. Cham, Switzerland: Springer, 2019.
[48] A. Bidram, F. L. Lewis, and A. Davoudi, "Distributed control systems for small-scale power networks: Using multiagent cooperative control theory," *IEEE Control Syst. Mag.*, vol. 34, no. 6, pp. 56–77, Dec. 2014.
[49] M. T. Hagan and M. B. Menhaj, "Training feedforward networks with the Marquardt algorithm," *IEEE Trans. Neural Netw.*, vol. 5, no. 6, pp. 989–993, Nov. 1994.
[50] E. Casagrande, W. L. Woon, H. H. Zeineldin, and D. Svetinovic, "A differential sequence component protection scheme for microgrids with inverter-based distributed generators," *IEEE Trans. Smart Grid*, vol. 5, no. 1, pp. 29–37, Jan. 2014.
[51] J. J. Q. Yu, Y. Hou, A. Y. S. Lam, and V. O. K. Li, "Intelligent fault detection scheme for microgrids with wavelet-based deep neural networks," *IEEE Trans. Smart Grid*, vol. 10, no. 2, pp. 1694–1703, Mar. 2019.

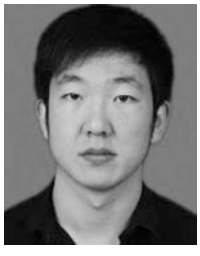

Zixiao Ma (Graduate Student Member, IEEE) received the B.S. degree in automation and the M.S. degree in control theory and control engineering from Northeastern University in 2014 and 2017, respectively. He is currently pursuing the Ph.D. degree with the Department of Electrical and Computer Engineering, Iowa State University, Ames, IA, USA. His research interests are focused on the power system load modeling, microgrids, nonlinear control, and model reduction.

Zhaoyu Wang (Member, IEEE) received the B.S. and M.S. degrees in electrical engineering from Shanghai Jiao Tong University in 2009 and 2012, respectively, and the M.S. and Ph.D. degrees in electrical and computer engineering from the Georgia Institute of Technology in 2012 and 2015, respectively. He is the Harpole-Pentair Assistant Professor with Iowa State University. His research interests include power distribution systems and microgrids, particularly on their data analytics and optimization. He is the Principal Investigator for a multitude of projects focused on these topics and funded by the National Science Foundation, the Department of Energy, National Laboratories, PSERC, and Iowa Energy Center. He is the Secretary of IEEE Power and Energy Society (PES) Award Subcommittee, the Co-Vice Chair of PES Distribution System Operation and Planning Subcommittee, and the Vice Chair of PES Task Force on Advances in Natural Disaster Mitigation Methods. He is an Editor of the IEEE TRANSACTIONS ON POWER SYSTEMS, the IEEE TRANSACTIONS ON SMART GRID, IEEE PES Letters, and the IEEE OPEN ACCESS JOURNAL OF POWER AND ENERGY, and an Associate Editor of *IET Smart Grid*.

Yifei Guo (Member, IEEE) received the B.E. and Ph.D. degrees in electrical engineering from Shandong University, Jinan, China, in 2014 and 2019, respectively.

He is currently a Postdoctoral Research Associate with the Department of Electrical and Computer Engineering, Iowa State University, Ames, IA, USA. He was a visiting student with the Department of Electrical Engineering, Technical University of Denmark, Lyngby, Denmark, from 2017 to 2018. His research interests include voltage/var control, renewable energy integration, distribution system optimization and control, and power system protection.

Yuxuan Yuan (Graduate Student Member, IEEE) received the B.S. degree in electrical and computer engineering from Iowa State University, Ames, IA, in 2017, where he is currently pursuing the Ph.D. degree. His research interests include distribution system state estimation, synthetic networks, data analytics, and machine learning.

Hao Chen (Member, IEEE) received the B.S. degree in electrical engineering from the Nanjing University of Science and Technology, Nanjing, China, in 2008, the M.S. degree in electrical engineering from the Illinois Institute of Technology, Chicago, in 2010, and the Ph.D. degree in electrical engineering from the Georgia Institute of Technology in 2016. From 2010 to 2012, he was an Electrical Engineer with Varentec, San Jose, CA, where he worked on various projects, including solid state transformers, dynamic VAr compensators, and voltage compensation for distribution system. He is currently a Staff Electronic Design Engineer with Tesla.